

PROPERTIES OF GLUON AND QUARK JETS

KLAUS HAMACHER

*Fachbereich Physik, Bergische Universität - Gh. Wuppertal, Gaußstraße 20, 42097 Wuppertal, Germany
DELPHI Collaboration*

E-mail: Klaus.Hamacher@cern.ch

Recent developments and results on the comparison of gluon to quark jets are discussed. A most important topic is the introduction of explicit energy scales of the jets. The scaling violation of the fragmentation function and the increase of the multiplicity with scale is shown to be directly proportional to the corresponding gluon or quark colour factor. The ratio of the hadron multiplicity in gluon to quark jets is understood to be smaller than the colour factor ratio due to differences in the fragmentation of the leading quark or gluon. Novel algorithms to reconstruct the colour portraits or the colour flow of an event are presented.

Talk given at the XXIX ICHEP, Vancouver, July 1998. A shortened version will appear in the conference proceedings.

1 Introduction

QCD contains two types of colour charged fields, quarks and gluons. The relative coupling strength of the quark gluon vertex and of the triple gluon vertex is determined by the QCD colour factors C_F and C_A . The values of the colour factors directly follow from the $SU(3)$ group structure of QCD. Reversely a precise measurement of the ratio of the couplings uniquely fixes the gauge group.

A basic prediction thus is that there should be about $C_A/C_F = 2.25$ times more gluon bremsstrahlung in gluon compared to quark jets¹. Scaling violation of the fragmentation function^{2,3} and the production of soft hadrons⁴ is correspondingly stronger in gluon jets.

The comparison of gluon and quark jets thus allows for basic and intuitive QCD tests. Moreover this comparison offers a direct handle on the fragmentation, the transition of colour charged fields into hadrons independent of fragmentation models.

Due to colour confinement there are, however, no free quarks and gluons. The definition of gluon and quark jets therefore relies on the analogy to tree level graphs. Corrections of order α_s/π have always to be expected. As QCD is a quantum theory also interference effects are anticipated due to the underlying event structure and due to the coherence of soft radiation. Both effects have indeed been observed. Finally effects due to the hadronic final state should be present. This is, however, part of fragmentation and what is to be understood. A final point of complication are the ambiguities introduced by the algorithms which are used to define the jets.

2 Experimental Topics and Energy Scales

The success of gluon and quark jet comparisons at LEP is due to two topics - the possibility of an unbiased tag of gluon jets and the better understanding of the (energy) scales underlying jet evolution.

Gluon jets were originally identified in (2- or 3-fold) symmetric three-jet (Y or *Mercedes*) events where two jets could be identified as (heavy) quark jets using impact parameter tags or energy ordering (see e.g.⁵). The remaining jet is then a gluon jet. A similar light quark

result can be obtained from a mixed quark/gluon sample from symmetric events by subtracting the gluon. Recently this technique has also been extended to non-symmetric topologies⁶. In this case one relies on the quark/gluon composition as predicted by the three-jet matrix element. The validity of this technique can, however, be tested by comparing results obtained with symmetric and non-symmetric events. This technique strongly improves the available statistic of gluon jets giving access to a much wider range of energy scales and allows so to compare the dynamics of gluon and quark jets.

A proper gluon to quark comparison has to be done with jets of a comparable scale. It turns out that this scale is not just the jet energy. The phase space for soft radiation is limited by coherence effects to cones given by the opening angles between the jets (angular ordering). The relevant scale thus is in general a product of jet energy E times opening angle θ i.e. a transverse momentum. This is what has originally been used in the so called MLLA (modified leading log approximation) calculations which were limited to small angles. If also larger opening angles are included it turns out that the so called hardness $\kappa = 2E \sin \theta/2$ is a better choice^{7,8}. This definition corresponds to an equivalent CMS energy. It should however be kept in mind that in multi-jet events several scales are relevant, in principle. In so far the usage of κ is an approximation which needs to be verified with data.

3 Results

3.1 Properties of Gluons at Fixed Scale

So far measurements observed gluon to quark multiplicity ratios in the range 1. to 1.5⁹. This low ratio has been ascribed to missing energy conservation in the theoretical calculations¹⁰. To minimise this effect as well as overlap effects between the jets it has been suggested¹¹ to study the most energetic gluons accessible at LEP, in events where the gluon recoils with respect to the $q\bar{q}$ -pair. The study of these rare events by OPAL¹² yields only 546 gluons from the total data set taken at the Z resonance. The average gluon energy is $\approx 42\text{GeV}$. The assignment of hadrons to the gluon is made inclusively: all hadrons

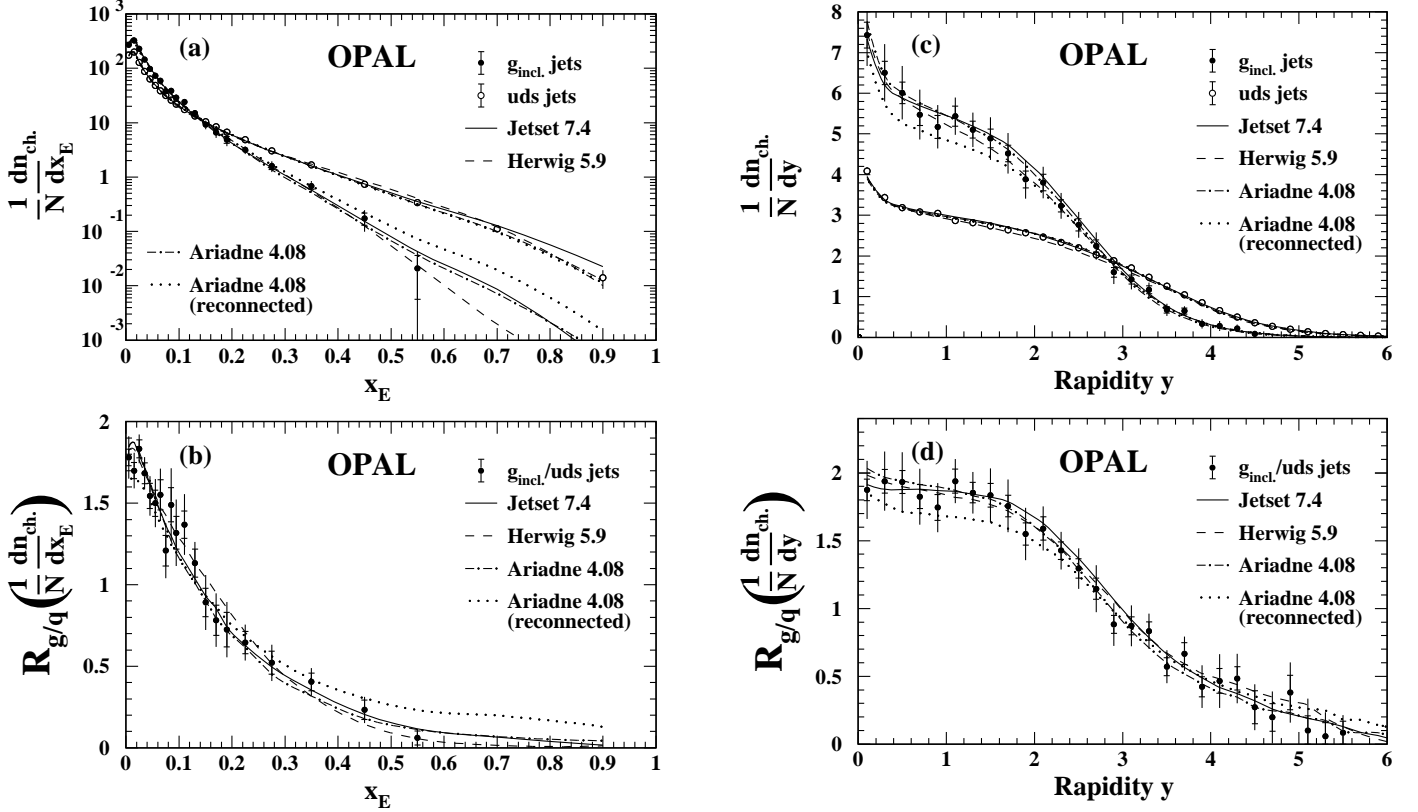


Figure 1: Gluon and quark fragmentation functions to charged hadrons as function of the scaled hadron energy x_E (a) and the rapidity y (c) with respect to the sphericity axis as measured by OPAL. The lower plots (b,d) show the gluon to quark ratio.

Table 1: Parameters of the gluon and quark multiplicity distributions measured by OPAL. $\langle N_{ch} \rangle$ is the mean charged multiplicity, D is the dispersion, γ is the skewness and c is the kurtosis.

	Gluon	Quark
$\langle N_{ch} \rangle$	$14.32 \pm 0.23 \pm 0.40$	$10.10 \pm 0.01 \pm 0.18$
D	$4.37 \pm 0.19 \pm 0.26$	$4.30 \pm 0.01 \pm 0.10$
γ	$0.38 \pm 0.13 \pm 0.18$	$0.82 \pm 0.01 \pm 0.04$
c	$0.18 \pm 0.34 \pm 0.30$	$0.98 \pm 0.03 \pm 0.11$

in the gluon hemisphere of the event are assigned to the gluon.

This selection proves to be robust against the usage of different cluster algorithms¹³. A comparison of these inclusive gluon-jets with identified uds quark jets yields multiplicity distributions with parameters given in Tab. 1. Skewness, kurtosis and multiplicity differ significantly between the gluon and quark distributions. If the slightly higher energy of the quark jets is considered by a Monte Carlo correction, even for these high energy gluons the multiplicity ratio still attains values much smaller than the simple QCD expectation¹²:

$$\frac{N_{ch}^{gluon}}{N_{ch}^{quark}} = 1.509 \pm 0.022 \pm 0.046 \quad (1)$$

A comparison of the gluon and quark factorial and cumulant moments has also been performed by OPAL. Cumulants K_q of order q measure the genuine q -particle

correlation. The predictions of these quantities¹⁴ were only found to agree “qualitatively” with the data¹². Partly this seems understandable as the leading order (LO), next to LO (NLO) and NNLO predictions differ strongly. A recent numerical calculation¹⁵ continuing the work of¹⁶, which now also considers energy conservation, the correct low energy behaviour as well as OPAL’s inclusive gluon jet definition, describes the data well.

Also charged hadron spectra have been studied for the inclusive gluons¹², see Fig. 1. Consistent with previous studies (see e.g.⁵) a roughly exponential falloff is observed for the distribution of the scaled charged hadron energy, x_E , which is more pronounced for gluons than for quarks. At large x_E the gluon distribution is suppressed with respect to the quark result by more than one order of magnitude, i.e. the production of fast, so-called leading particles is strongly suppressed in gluon jets. At the smallest x_E , however, the gluon to quark ratio reaches values of up to 1.8. The distribution of the rapidity with respect to the sphericity axis of the event shows a corresponding behaviour. This choice of the observable “zooms” the range of low hadron energies. At the smallest rapidities ($y < 2$) a high gluon to quark ratio is observed as expected in¹⁷:

$$\frac{dN_{ch}^{gluon}/dy}{dN_{ch}^{quark}/dy} = 1.815 \pm 0.038 \pm 0.062 \quad (2)$$

Although not mentioned in¹² it is important to note that in the rapidity range $3 \leq y \leq 6$ the gluon distribution

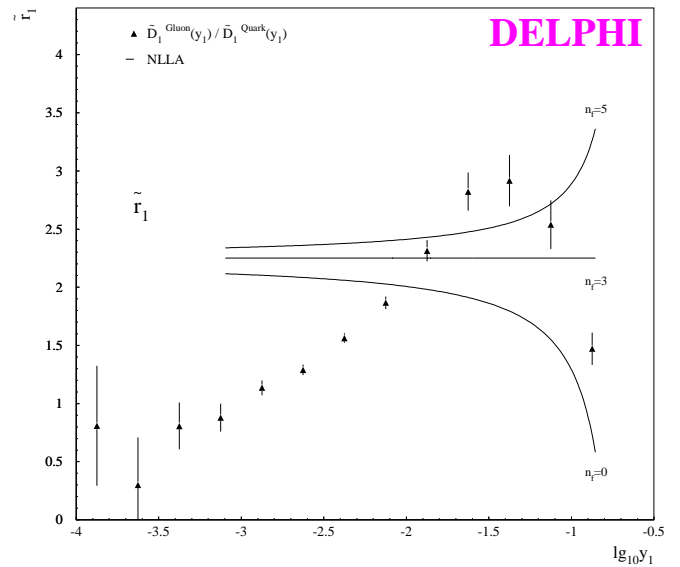
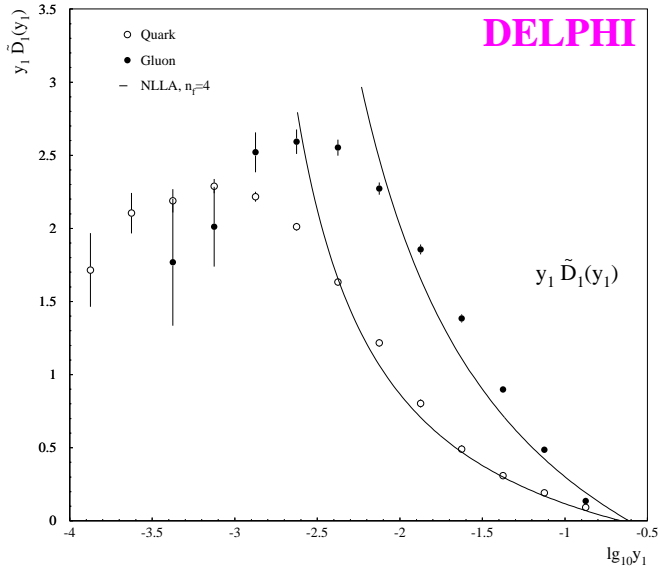


Figure 2: Gluon and quark splitting kernels (left) and their ratio (right) as measured by DELPHI. Theoretical expectations are shown as lines.

is below the quark distribution. The area between the gluon and the quark distribution amounts to almost one unit of charged multiplicity. This suppression further extends down to rapidities of $y \sim 2$ as is observed from Fig. 1d) and necessarily needs to be taken into account when comparing the QCD expectation for the gluon to quark multiplicity ratio to data, e.g. for Eqn. 1.

In order to verify the QCD prediction of a stronger splitting probability for gluons and also to clarify the origin of the small observed multiplicity ratio DELPHI directly measured the so-called splitting kernels. These are the most important piece of the evolution equations for the generating functions or functionals which describe the jet- and hadron multiplicities (see e.g. 7). The importance of these kernels, commonly known is the special (collinear) case of the Altarelli-Parisii kernels, can be understood from the following simplified argumentation². Consider a given number of partons $N_1(y)$ which have not split (or decayed) at a given jet resolution y . The number of partons which will split in an interval Δy then is expected to be:

$$\begin{aligned} \Delta N_1(y) &= -F(y) \cdot N_1(y) \cdot \Delta y \implies \\ F(y) &= -\frac{1}{N_1(y)} \cdot \frac{dN_1(y)}{dy} \end{aligned} \quad (3)$$

This equation is analogous to the radiative decay equation, however, with a y dependent decay “parameter” $F(y)$ describing the dynamics of the process. This is the splitting kernel. Eqn. 3 can be expressed by the usual jet rates $R_n = N_n/N_{tot}$ and then yields:

$$-F(y) = \tilde{D}_1(y) \approx \frac{d \log R_1(y)}{dy} \quad (4)$$

In analogy to the differential jet rates known from the α_s analyses, the quantity $\tilde{D}_1(y)$ is called modified differential 1-jet rate. It is a direct experimental measure of the splitting kernel.

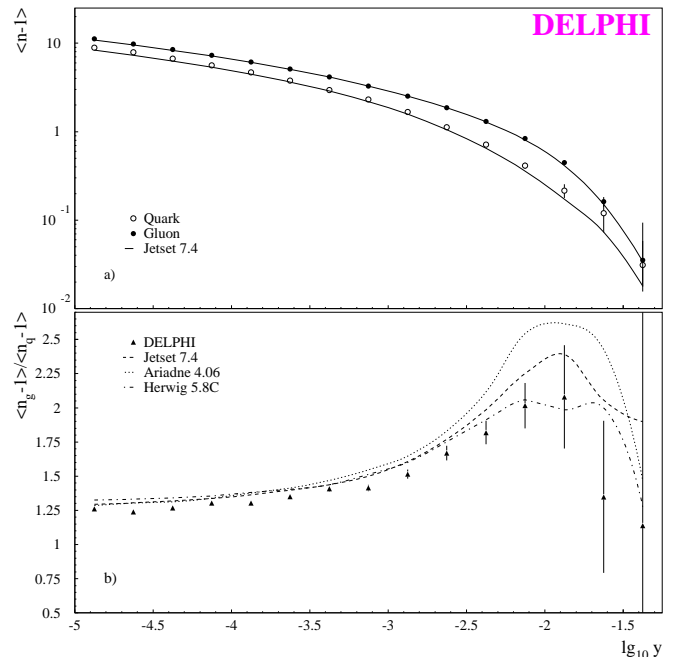


Figure 3: Average subject multiplicity minus 1 for gluon and quark jets (upper plot) and gluon to quark ratio (lower plot) as function of the resolution y .

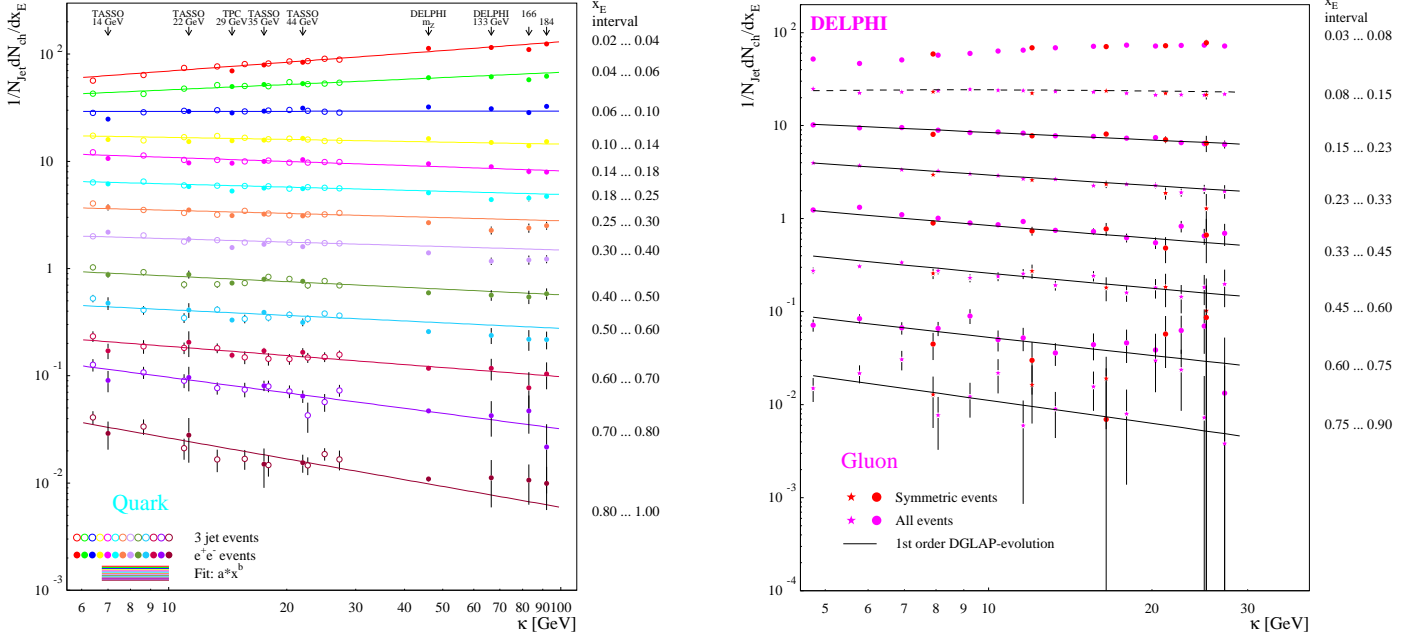


Figure 4: Left side: Scale dependence of the quark fragmentation function measured in three-jet events as function of the hardness scale κ compared to measurements in e^+e^- annihilation. Lines are power fits to the three-jet data. Right side: Scale dependence of the gluon fragmentation function measured in 3 jet events as function of the hardness scale κ . Data points belong to symmetric and non-symmetric topologies. Lines result from a simultaneous DGLAP fit of the gluon and quark fragmentation function.

The result of the DELPHI measurement for gluons and quarks as function of y as defined with the Durham algorithm⁸ as well as the corresponding ratio is shown in Fig. 2. At large y the data about follow the perturbative expectation. A deviation at very large y (best seen in the gluon to quark ratio) is due to the structure of the underlying three-jet events² (see also behaviour of the subjet multiplicity-1 in¹⁸). The gluon and the quark cannot be treated as independent objects in this limit as the large y splitting resolves the underlying event. At smaller y both the quark and the gluon data fall below the perturbative expectation. This is to be expected due to non-perturbative hadronization effects. It is most important, that this influence sets in already at larger y (i.e. “earlier”) for gluons compared to quarks. This causes the initially large gluon to quark ratio to fall off rapidly with falling y .

In the framework of the HERWIG cluster fragmentation model¹⁹ this effect can easily be understood. Quarks are valence particles of hadrons whereas gluons are not. Gluons have to be split into a $q\bar{q}$ -pair first. So hadronization effects should be visible already at larger y in case of gluons. The same effect is responsible for the suppression of the fragmentation function at large x_E or large rapidity y as discussed above.

The behaviour of the so called sub-jet multiplicity $\langle n_{jet} \rangle = \sum_i i \cdot R_i$ (see Fig. 3a)) illustrates that this is indeed the reason for the gluon to quark multiplicity ratio to be smaller than expected. Initially at $\log y \approx -2$ the subjet multiplicity-1 ratio^a (see Fig.3b) reaches about the expected value ≈ 2 . Then in coincidence with the

^a1 is subtracted to consider the initially present parton.

deviation of $\tilde{D}_1^g(y)$ from the perturbative expectation this ratio falls off and rapidly reaches values typical for the hadronic multiplicity ratio. Note from Fig. 3a) that this happens when the typical subjet multiplicities are around 3, thus at much larger y than most hadrons are formed.

3.2 Scale Dependence of Quark and Gluon Fragmentation

DELPHI in several publications^{2,3,4,5} attempted to compare the scale dependence thus the dynamical evolution of gluons and quarks. Using the full data set containing about 85000 identified gluon jets a detailed comparison of the gluon and quark fragmentation function $D(x_E)$ as function of κ is performed³. The measurement is shown in Fig. 4. The quark fragmentation function as obtained from quark jets in three-jet events (left side) was fitted by a power ansatz superimposed to the data (open points). Also shown (full points) is the fragmentation function as measured in e^+e^- annihilation from PETRA energies²⁰ up to the highest LEP energies. Both measurements agree very well, enforcing the interpretation of κ as a valid scale for jet evolution in three-jet events. It should, however, be mentioned that the transverse momentum of a jet with respect to the event axis works similarly well. The corresponding result for gluons is shown on the right side of Fig. 4. Results for symmetric and for all topologies agree well, strengthening again the validity of the analysis and the scale. The fits shown with the scale dependence of the gluon fragmentation function result from a simultaneous 1st order DGLAP evolution together with the quark fragmentation function. The strong coupling, the colour factor ratio C_A/C_F , as well as the parameters

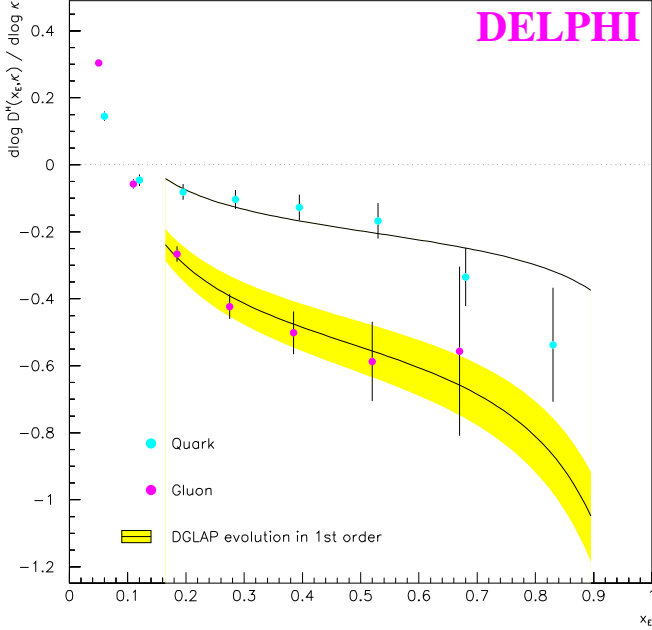


Figure 5: Slopes of the scale dependence of the quark and gluon fragmentation function as function of x_E . The shaded area indicates the stat. uncertainty of C_A from the DGLAP fit. Data points result from power law fits of the individual x_E intervals.

of the analytic ansatz of the fragmentation functions were treated as free parameters. The fit yields the following preliminary result for the colour factor ratio:

$$\frac{C_A}{C_F} = 2.44 \pm 0.21(stat.) \quad (5)$$

Fig. 5 compares the logarithmic slope of the gluon and quark fragmentation function as function of x_E . The function is the result of the DGLAP fit of the data. The shaded area indicates the uncertainty on C_A for fixed $C_F = 4/3$. The data points were obtained from power law fits to each gluon and quark x_E interval individually. As expected from the structure of the DGLAP equation scaling violations are much stronger for gluons than for quarks^b. Due to the stronger scaling violations in gluon jets $p\bar{p}$ scattering which is dominated by gluon-gluon scattering should be well suited to measure α_s from the scaling violation of the charged hadron fragmentation function.

It is evident from the gluon to quark comparison at low x_E - indicating a ratio of about 2 (see Fig. 5) - that the scale dependence of the hadron multiplicity opens a new way in testing the prediction:

$$\frac{\langle N_{ch}^{gluon} \rangle}{\langle N_{ch}^{quark} \rangle} \cong \frac{C_A}{C_F} \quad (6)$$

insensitive to the non-perturbative effects discussed above. Note that the prediction Eqn. 6 is expected to be valid for any large scale if non-perturbative effects can

^bNote that the Altarelli-Parisi splitting functions include the individual colour factors multiplicatively.

be neglected. Consequently also the ratio of the derivative of the multiplicities with respect to the relevant scale (here taken to be κ) is equal to the colour factor ratio:

$$\frac{\partial \langle N_{ch}^{gluon}(\kappa) \rangle / \partial \kappa}{\partial \langle N_{ch}^{quark}(\kappa) \rangle / \partial \kappa} = \frac{C_A}{C_F} \quad (7)$$

This prediction is equivalent to Eqn. 6 but, as the multiplicity evolves slowly with scale, should hold already at much smaller scale. The comparison of the gluon and quark splitting kernels as well as the behaviour of the fragmentation function suggest that most of the non-perturbative difference between gluons and quarks is due to the fragmentation of the leading quark or gluon, thus is to be expected to happen at very small scale. A corresponding calculation in the framework of the colour dipole model²¹ confirms this expectation.

Fig. 6 compares the dependence of the multiplicity assigned to gluon and quark jets as function of $\log \kappa$. It is immediately evident from this plot that the slope of the gluons is roughly twice as big as for quarks thus already impressively confirming the QCD expectation Eqn. 7. The data was fit with the predictions for the evolution of the multiplicity with scale as given in^{22,23}, however, adding constant terms to account for non-perturbative differences between gluons and quarks, thus:

$$\begin{aligned} \langle N_{ch}^q(\kappa) \rangle &= \langle N_{ch}^{perturb.}(\kappa) \rangle \cdot N_0^q \\ \langle N_{ch}^g(\kappa) \rangle &= \langle N_{ch}^{perturb.}(\kappa) \rangle \cdot r_{gq}(\kappa) + N_0^g \end{aligned} \quad (8)$$

$r_{gq}(\kappa)$ is a NNLO prediction for the multiplicity ratio as given in²⁴. The ansatz represents the data well. The resulting colour factor ratio is:

$$\frac{C_A}{C_F} = 2.14 \pm 0.10(stat.) \quad (9)$$

No systematic error is given with this measurement as a superior method is discussed also in⁴ which determines the colour factor ratio from the scale dependence of the multiplicity of three-jet events. It is insensitive to ambiguities induced by the choice of the scale and also accounts for coherent radiation from a $q\bar{q}g$ - ensemble (see also²⁵). The non-perturbative term introduced in this study which accounts for differences in the fragmentation of the primary quark or gluon is $N_0^q - N_0^g = 1.97 \pm 0.03 \pm 0.33$.

It is instructive to estimate a lower limit for $N_0^q - N_0^g$ from the gluon and quark fragmentation functions² in the momentum range where the gluon is below the quark fragmentation function (compare also Fig.1a,c)). This limit can be calculated by subtracting the observed gluon multiplicity from the (wrongly) expected one: $N_g^{expected} \approx 2N_q$. This yields $N_0^q - N_0^g > 1.22 \pm 0.08 (> 1.15 \pm 0.2)$ from *Y* and *Mercedes* events, respectively. As the suppression persists to lower x_E or y (see Fig. 1b,d)) it probably amounts for the full non-perturbative term $N_0^q - N_0^g$.

The left side of Fig. 6 presents the gluon to quark multiplicity ratio, the ratio of the fitted functions Eqn.

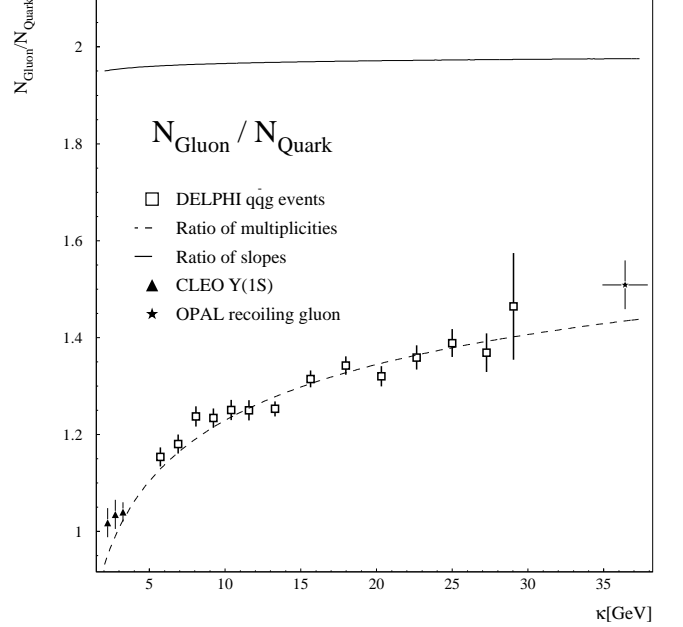
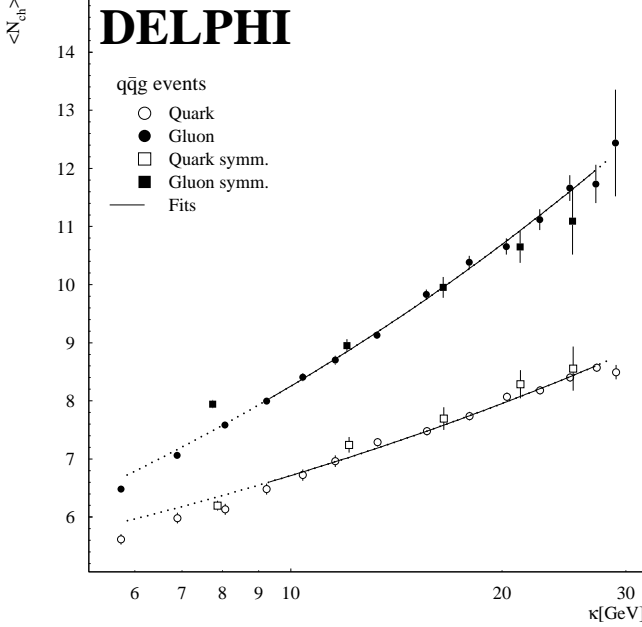


Figure 6: Left: Scale (κ) dependence of the jet multiplicity in gluon and quark jets as measured by DELPHI. Lines are the result of a fit of Eqn. 7 Right: Ratio of the gluon to quark multiplicity as function of the scale. The lower line is the ratio of the fits on the right. The upper line is the ratio of the slopes of these fits.

8 as well as the corresponding slope ratio. Also included are measurements at very small scale (4-7 GeV) performed by CLEO²⁶ in $\Upsilon(1S) \rightarrow gg\gamma$ decays and the OPAL result for inclusive gluons. For this point κ has been estimated from the average gluon energy and the angle cuts given in¹². As this result compares gluon to pure light quark (uds) jets it may be expected to lie slightly higher than the extrapolation of the DELPHI result. The fit describes all measurements well, confirming that the non-perturbative effects can be absorbed effectively into constant terms allocated to the leading particles in a quark or gluon jet.

3.3 Reconstruction of Colour Connections

The stronger radiation off a gluon may also be interpreted as due to two colour connections compared to one in the case of quarks. One may then try to reconstruct the colour connections in an event to distinguish e.g. 4 quark final states (like $WW \rightarrow q\bar{q}q\bar{q}$ events, 2 connections) from QCD background ($q\bar{q}gg$, 3 connections). One may also try to reduce the combinatorial background in combining only the colour connected $q\bar{q}$ -pairs in WW events. Besides several theoretical proposals related to this subject²⁷ now first experimental results are available^{28,29}. These are based on the idea of reconstructing the colour portrait of a process³⁰. To introduce the algorithm recall first the structure of the soft hadron (labeled h) production cross-section in a hard n parton (labeled i, j) initial state^{31,32}:

$$d\sigma_h^{soft} \propto d\sigma^{hard} \cdot \alpha_s \cdot d\Omega \cdot \frac{dE_h}{E_h} \sum_{i,j \text{ hard}}^n C_{ij} \cdot W_{ij}$$

$$W_{ij} = \frac{\sin^2\theta_{ij}/2}{\sin^2\theta_{ih}/2 \cdot \sin^2\theta_{jh}/2} \quad (10)$$

Important pieces in this equation are the colour factors C_{ij} which contain the information about the colour connections ($C_{ij} = 0$ if no connection) and the so called antenna pattern W_{ij} which determine the angular structure of the radiation. The poles $\theta_{kh} \rightarrow 0$ appear in the direction of the hard partons and lead to the formation of the jets. The nominator contains the angular dependence known from the hardness scale. The idea is to reconstruct the colour connections by adequately weighting the observed soft hadron production. The algorithm proceeds as follows:

- Reconstruct jet directions from leading particles.
- Calculate the probability for un-associated (low energy, large angle) particles to stem from a cluster (hard parton) j :

$$w_{hj} = \frac{C_j}{k_{hj}^2} = \frac{C_j}{2E_h^2 \sin^2\theta_{hj}/2} \quad (11)$$

Renormalise so that $\sum w_{hj} = 1$.

- Associate hadron h to the cluster pair which maximises $w_{hkl} = w_{hl} + w_{hk}$. Calculate the colour connection coefficient:

$$W_{kl} = C \sum_{h \text{ assoc.}} g(E_h) \cdot w_{hkl} \quad (12)$$

$g(E_i)$ is an energy dependent weight, C is chosen so to properly normalise the W_{kl} ; $\sum W_{kl} = 2$.

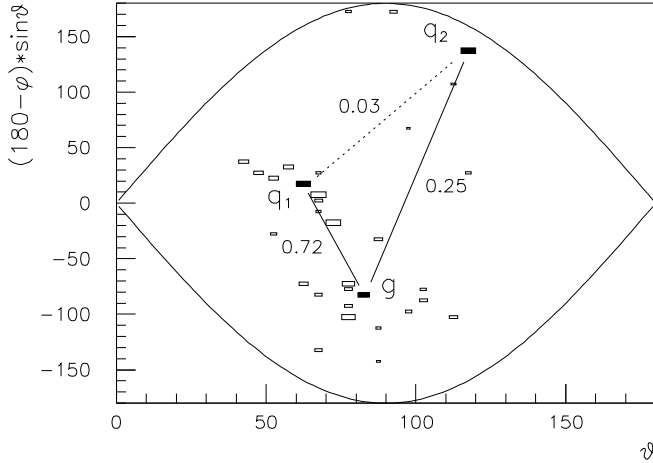


Figure 7: Fish-eye plot of the hadron distribution in a typical *Mercedes* event (Monte Carlo).

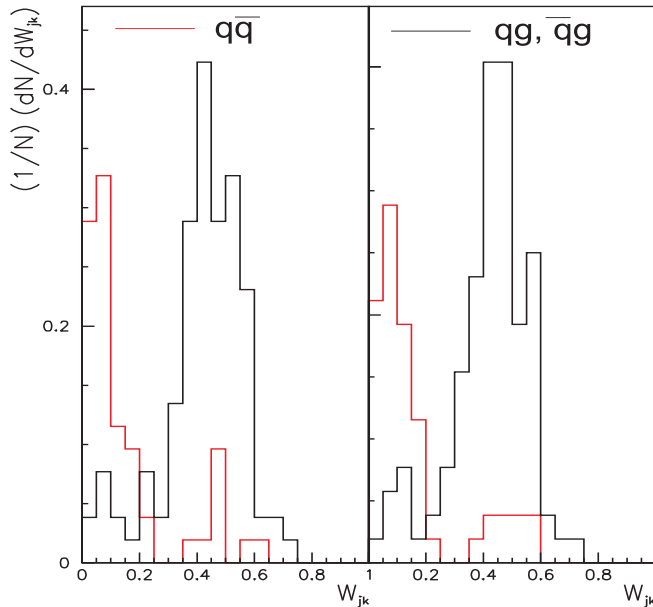


Figure 8: Weight distribution for *Mercedes* events (DELPHI data).

To test the technique it has been applied to *Mercedes* events (Monte Carlo and data) where the (heavy) quark jets were additionally identified using an impact parameter tag²⁸. Fig.7 shows a typical event. It is clearly observed that the soft hadrons (boxes) accompany the quark-gluon colour connections indicated by the lines. The corresponding colour connection coefficients clearly distinguish the $qg(\bar{q}g)$ from the $q\bar{q}$ case. Fig. 8 (left) shows the colour connection coefficients which were obtained from DELPHI events of the *Mercedes* topology. The additional impact parameter identification allows to measure directly the purity and efficiency of the algorithm. The data show that purities of 90% at 80% efficiency can be obtained.

A modification of the algorithm has also been applied to the analysis of $WW \rightarrow q\bar{q}q'\bar{q}'$ events at 189 GeV centre-of-mass energy measured by DELPHI. As proposed in³³ all (hypothetical) strings connecting the

4 parton final state were boosted to their rest systems. Then the transverse momentum of the hadrons with respect to the string was calculated and similar to Eqn. 11 weights were defined using the transverse momentum of the hadrons $w_{hj} = C_h/p_t^h$. The string configuration which minimises the sum of the transverse momenta was selected. Fig. 9 shows the mass spectrum of all possible jet-jet pairs (upper plot) and taking only the combinations selected by the algorithm outlined above. A clear reduction of the combinatorial background due to wrong $q\bar{q}'$ pairing is indicated. Contrary to kinematic cuts the method does not bias the W -mass. So far no attempt has been made to reject QCD background. Thus the appeared reduction of this contribution is due to the reduced combinatoric only. Currently the method can only be used as an additional tool as the efficiency is only about 50%. Improvements are however to be expected in the near future.

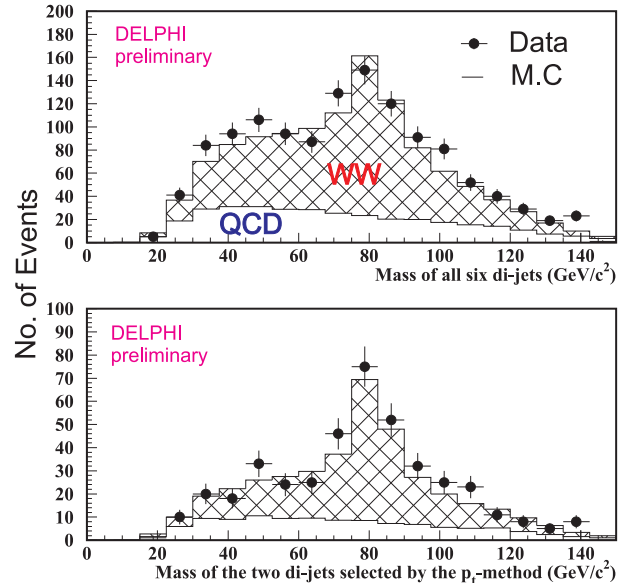


Figure 9: Jet-jet mass distribution for four-jet events measured by DELPHI at 189 GeV. The upper plot contains all combinations, the lower only those selected with the algorithm described in the text. Histograms indicate the Monte Carlo predictions for WW and QCD events.

4 Summary

The introduction of energy scales in the comparison of gluon and quark jets opened the possibility for studies of the scale dependence of gluon and quark jet properties. This in turn lead to the understanding of the (smaller than originally expected) gluon to quark multiplicity ratio due to non-perturbative effects in the fragmentation of the leading gluon or quark and to the possibility to really measure the colour factor ratio from a direct gluon to quark jet comparison. These observations will soon be further exploited in order to identify quark and gluon jets or colour connections in multi-jet environments.

Acknowledgements

I would like to express my gratitude to the colleagues who provided me with input for this talk: B. Gary, A. Kiiskinen, S. Lupia, V. Nomokonov and R. Orava. Especially I like to thank O. Klapp, P. Langefeld and M. Siebel for their persistent effort and the pleasant time during the gluon analysis of the Wuppertal group of DELPHI.

References

1. S.J. Brodsky and J.F. Gunion, *Phys. Rev. Lett.* **37**, 402 (1976), K. Konishi, M. Massoth, A. Ukawa and G. Veneziano, *Phys. Rev. Lett.* **78**, 243 (1978).
2. DELPHI Collab., P. Abreu et al., *Eur.Phys.J. C* **4**, 1-17 (1998).
3. DELPHI Collab., K. Hamacher, O. Klapp, P. Langefeld, M. Siebel et al., Contrib. Paper 147 to the XXIX ICHEP, Vancouver, 1998.
4. DELPHI Collab., K. Hamacher, O. Klapp, P. Langefeld, S. Martí, M. Siebel et al., Contrib. Paper 146 to the XXIX ICHEP, Vancouver, 1998.
5. DELPHI Collab., P. Abreu et al., *Z. Phys. C* **70**, 179 (1996)
6. M. Siebel, Diplomarbeit, Bergische Univ.-Gh. Wuppertal, WUB-DI 97-43 (1997).
7. V. A. Khoze and W. Ochs, *Int.J.Mod.Phys.A* **12**, 2949 (1997).
8. S. Catani et al., *Phys. Lett. B* **269**, 432 (1991).
9. See⁵, a compilation including other results is given in: J. Fuster et al. in Proc. of QCD 96, Montpellier, 1996, *Nucl. Phys. B* (Proc. Suppl.) **54a**, 1997 (.)
10. OPAL Collab., G. Alexander et al., *Phys. Lett. B* **388**, 659 (1996);
11. B. Gary, *Phys. Rev. D* **49**, 4503 (1994).
12. OPAL Collab., Contrib. Paper 378 to the XXIX ICHEP, Vancouver, 1998.
13. OPAL Collab., K. Ackerstaff et al., *Eur.Phys.J. C* **1**, 479 (1998).
14. I.M. Dremin and R.C. Hwa, *Phys. Rev. D* **49**, 5805 (1994).
15. S. Lupia, MPI-PhT/98-49 (1998), Contrib. Paper to the XXIX ICHEP, Vancouver, 1998.
16. S. Lupia and W. Ochs, MPI-PhT/97-46 (1997), MPI-PhT/97-72 (1997), Contrib. Papers to the XXIX ICHEP, Vancouver, 1998.
17. S. Catani, Jet Physics at LEP and SLC, Johns Hopkins Workshop, Florence, Italy, 31 Aug - 2 Sep 1994, hep-ph/9411361.
18. ALEPH Collab, R. Barate et al., CERN-EP/98-16.
19. G. Marchesini and B.R. Webber, *Nucl. Phys. B* **283**, 1 (1984), B.R. Webber, *Nucl. Phys. B* **283**, 492 (1984).
20. TASSO Collab., W. Braunschweig et al., *Z. Phys. C* **45**, 193 (1989)
21. P. Edén, LU-TP 98-11 (1998) and hep-ph/9805228.
22. Yu. L. Dokshitzer, V.A. Khoze and S.I. Troyan, *Int.J.Mod.Phys.A* **7**, 1875 (1992)
23. B.R. Webber, *Phys. Lett. B* **143**, 501 (1984)
24. J. B. Gaffney and A.H. Müller *Nucl. Phys. B* **250**, 501 (1985)
25. R. Ströhmer, to appear in Proceedings of the XXIX ICHEP, Vancouver, 1998.
26. CLEO Collab., M.S. Alam et al., *Phys. Rev. D* **56**, 17 (1997)
27. J. Ellis, V.A. Khoze and W.J. Stirling, *Z. Phys. C* **75**, 287 (1997); A. Heyssler, V.A. Khoze, W.J. Stirling, CERN-TH-98-150; V.A. Khoze and T. Sjöstrand, CERN-TH-98-74.
28. DELPHI Collab., M. Battaglia, A. Kiiskinen, V. Nomokonov, R. Orava et al., Contrib. Paper 150 to the XXIX ICHEP, Vancouver, 1998.
29. DELPHI Collab., A. Kiiskinen, V. Nomokonov, R. Orava et al., Contrib. Paper 151 to the XXIX ICHEP, Vancouver, 1998.
30. R. Orava et al., HIP-1997-66-EXP, Contrib. Paper to the XXIX ICHEP, Vancouver, 1998.
31. Ya.I. Azimov, Yu.L. Dokshitzer, V.A. Khoze, S.I. Troyan, *Phys. Lett. B* **165**, 147-150 (1985).
32. R.K. Ellis, W.J. Stirling and B.R. Webber, QCD and Collider Physics, Cambridge Univ. Press, 1996.
33. E. Norrbin and T. Sjöstrand, *Phys. Rev. D* **55**, 1 (1997)